ResearchGate

See discussions, stats, and author profiles for this publication at: https://www.researchgate.net/publication/267983923

Electronically Nonadiabatic Decomposition Mechanisms of Clusters of Zinc and Dimethylnitramine

ARTICLE *in* CHEMICAL PHYSICS · NOVEMBER 2014

Impact Factor: 1.65 · DOI: 10.1016/j.chemphys.2014.11.003

READS

153

3 AUTHORS, INCLUDING:

Anupam Bera

Indian Institute of Science

2 PUBLICATIONS **0** CITATIONS

SEE PROFILE

Atanu Bhattacharya

Indian Institute of Science

20 PUBLICATIONS **275** CITATIONS

SEE PROFILE

All in-text references underlined in blue are linked to publications on ResearchGate, letting you access and read them immediately.

Available from: Anupam Bera
Retrieved on: 23 January 2016

Chemical Physics 446 (2015) 47–56

Contents lists available at ScienceDirect

Chemical Physics

journal homepage: www.elsevier.com/locate/chemphys

Electronically nonadiabatic decomposition mechanisms of clusters of zinc and dimethylnitramine

Anupam Bera, Sonal Maroo, Atanu Bhattacharya *

Department of Inorganic and Physical Chemistry, Indian Institute of Science, Bangalore 560012, India

ARTICLE INFO

Article history:
Received 12 August 2014
In final form 2 November 2014
Available online 7 November 2014

Keywords:
Unimolecular decomposition
CASSCF calculation
Metal-nitramine
ONIOM-CASSCF

ABSTRACT

Electronically nonadiabatic decomposition mechanisms of dimethylnitramine (DMNA) in presence of zinc metal clusters are explored. Complete active space self-consistent field (CASSCF) calculation is employed for DMNA–Zn and ONIOM (Our own N-layered integrated molecular orbital and molecular mechanics) methodology is coupled with CASSCF methodology for DMNA–Zn_{10} cluster. Present computational results show that DMNA–Zn clusters undergo electronically nonadiabatic reactions, rendering nitro-nitrite isomerization followed by NO elimination. The overall reactions are also found to be highly exothermic in nature. This is the first report on electronically nonadiabatic decomposition pathways of DMNA–Zn_n neutral clusters.

© 2014 Elsevier B.V. All rights reserved.

1. Introduction

Energetic materials encompass substances (composed of organic molecules containing C, H, N, and O) that are potent sources of large chemical energy which is released upon their rapid decomposition or detonation. They constitute a major part of propellants, explosives, and pyrotechnics and their applications span over a wide region from mining, construction and demolition to safety equipments (signal flares and fire suppression systems), rocketry and space exploration. It is because of their great practical importance that researches are being carried out to understand and to optimize the performance, burning behavior, stability, and detonation properties [1–3]. The focus is often laid on quantifying the amount of energy released, identifying key reaction mechanisms, or investigating ways in which the energy release can be controlled. In order to accomplish these tasks, however, we must understand the fundamental steps in the overall decomposition of energetic materials. Even the initial steps in the overall decomposition of energetic molecules are complex, involving numerous chemical and physical events in a concerted and synergistic fashion, often influenced by a variety of factors. If the dissociation/detonation of energetic materials is initiated by sparks, shock waves or arcs then the decomposition can begin with promoting energetic molecules to the electronically excited states [4]. For an example, recent *ab initio* calculations show that shock compression at a pressure of 30 GPa or above can cause an electronic excitation equivalent to 2–5 eV [4e], which is comparable to the excitation energies of the low lying excited electronic states of most of the energetic molecules, such as RDX, HMX, CL-20 [5]. Recently, Bernstein and his co-workers have firmly established, both theoretically and experimentally, that conical intersections, which create a funnel-like topography of potential energy surfaces (PESs) due to the crossing of multidimensional electronic PESs, are a controlling factor in the excited electronic state decomposition of energetic molecules [6]. Thus, the initial decomposition steps of the energetic molecules are electronically non-adiabatic in nature, because of the involvement of more than one electronic PES.

For a long time, molecular energetic materials, which are composed of oxidizer and fuel in one molecule such as RDX, HMX, CL-20, were used as rocket propellants for their ability to release high energy during decomposition or detonation; however, recently, metalized energetic materials, which are the mixture of these molecular energetic materials and metal particles (e.g., Zn, Al, Fe, etc.), are found to be better propellants over molecular energetic systems. The efficiency of energy release of metalized energetic materials is twice as compare to the best molecular energetic materials [7], shortening the ignition delay time with complete combustion, faster energy release and more control over performance [8]. There is a wide consensus in the energetic materials community that this increase in efficiency of the energy release by metalized energetic materials is attributed to the exothermicity of stable oxide formation of the corresponding metal (e.g., heat of oxide formation for aluminium ($4Al + 3O_2 \rightarrow 2Al_2O_3$) is −1676 kJ/mol [9] and that for zinc ($2Zn + O_2 = 2ZnO$) is −347 kJ/mole [10]). But this explanation is not just sufficient

* Corresponding author.
E-mail address: atanub@ipc.iisc.ernet.in (A. Bhattacharya).

http://dx.doi.org/10.1016/j.chemphys.2014.11.003
0301-0104/© 2014 Elsevier B.V. All rights reserved.

enough to explain all the other important noticeable behaviors of the metalized energetic materials over the molecular ones. Is there any other effect of metal surfaces and particles in the overall excited electronic state decomposition mechanisms of metalized energetic materials? Are the excited electronic state decomposition mechanisms of molecular energetic materials altered in presence of metal particles? These questions remain in literature mostly unanswered, so far. To address these questions, it is essential to obtain detailed knowledge about the electronically nonadiabatic decomposition mechanisms of the energetic molecules in presence of metal particles. Furthermore, as excited electronic states play an important role in the decomposition of energetic materials, it is also relevant to explore the excited electronic state potential energy surfaces of energetic molecules in presence of metal atoms and clusters.

Nitramine (N–NO_2) energetic molecules, such as RDX, HMX and CL-20, which are well-known molecular energetic systems, usually contain a number of N–NO_2 moieties. Each moiety, however, is not connected by π-conjugation and therefore, they can be viewed as chemically isolated energetic sites. As nitramine energetic molecules are large and chemically complex, a rather structurally simple analogue molecule, dimethyl nitramine (DMNA, containing one N–NO_2 moiety) has been subjected to laboratory-based detailed experimental and theoretical study [11], for a long time. These studies unravel intrinsic decomposition behavior of the nitramine moiety. To date, electronically nonadiabatic decomposition of isolated DMNA has been investigated experimentally and theoretically, in details [11]. Bhattacharya et al. provided the valuable insights on the decomposition mechanisms of DMNA following its electronic excitation both experimentally and theoretically [11a]. Isolated DMNA exhibits nitro-nitrite isomerization followed by NO elimination and these initial decomposition steps are found to be endothermic in nature. Recently, we have explored the excited electronic state surfaces of DMNA in presence of Al clusters [12], which clearly reveals that presence of Al metal atom brings about significant changes in the electronically nonadiabatic decomposition pathways of DMNA. While the isolated DMNA shows endothermic initial reaction steps, DMNA–Al clusters exhibit exothermic reaction steps. Following this DMNA–Al study, in the present work, we have explored the excited electronic state surfaces of clusters of DMNA and Zinc (Zn).

Recent thermal decomposition study of RDX (containing three N–NO_2 moiety) molecules in presence of Zn nanoparticles [8] features that addition of zinc nanoparticles to RDX reduces the ignition delay time by 20%, triples the temperature and decreases the emergence time of the products by 10–40%. The excited electronic state decomposition mechanisms of nitramine energetic molecules in presence of various Zn metal clusters, however, have not been explored yet, both experimentally and theoretically. To address the role of Zn metal in the overall electronically nonadiabatic decomposition mechanisms of one nitramine (N–NO_2) moiety, we have selected two different systems, namely, DMNA–Zn and DMNA–Zn_{10} and have explored the excited electronic state surfaces of these two clusters. For the present study, we have chosen Zn_{10} cluster because a recent DFT study on the structures and electronic states of zinc clusters (Zn_n, n = 2–32) identifies Zn_{10} as one of the most stable clusters formed by zinc. Its stability is attributed to its high binding energy and shorter bond length [13]. For DMNA–Zn cluster we have employed complete active space self-consistent field (CASSCF) calculations to explore its excited electronic state surfaces. For DMNA–Zn_{10} cluster, on the other hand, a hybrid methodology, called Our Own N-layered Integrated Molecular Orbital and Molecular Mechanics (ONIOM), which was originally developed by Morokuma and co-workers [14], is employed. In ONIOM methodology, DMNA along with one Zn atom is placed at high layer, which is treated with CASSCF methodology, while remainder of the Zn_{10} cluster is treated with universal force field (UFF) molecular mechanics and Møller–Plesset second order perturbation (MP2) theory. In order to incorporate dynamic correlation in CASSCF calculations we have employed single point CASMP2 [15] calculations. Present computational results reveal that DMNA–Zn exhibits N–N bond dissociation, followed by Zn–O bond dissociation, which finally leads to nitro-nitrite isomerization followed by NO elimination. DMNA–Zn_{10} also shows N–N bond dissociation followed by isomerization; however, one intermediate, which is present in the overall decomposition of DMNA–Zn following electronic excitation, does not take part in that of DMNA–Zn_{10}. In the present work, exothermicities associated with the overall decomposition reaction for DMNA–Zn and DMNA–Zn_{10} clusters are also examined.

2. Theoretical procedure

All geometry optimizations at the ground and excited electronic states of DMNA–Zn are performed at the complete active space self-consistent field (CASSCF) level of theory with 6-31G(d) basis set (denoted as CASSCF/6-31G(d)) using Gaussian 09 [16]. In the CASSCF method, multiconfiguration wave function is variationally optimized with respect to simultaneous variations of the orbitals and configuration coefficients; however, all possible configuration state functions (CSFs) are prepared based on the active orbitals, which comprise active space in the CASSCF calculation. The active orbitals, used in the CASSCF calculation for DMNA–Zn, are depicted in Fig. 1. The active space comprises 14 electrons distributed in 11 orbitals, denoted as CASSCF(14,11). The orbitals are selectively chosen to include all the important bonding, nonbonding and antibonding orbitals in N–NO_2–Metal active moiety. Thus, the orbitals used for DMNA–Zn include σ_{ONO}, $n\sigma_O$, π_{ONO}, $n\sigma_O$, σ_{ONO}, $5S_{Zn}$, nd_{Zn}, σ^*_{ZnO}, π^*_{ONO}, σ^*_{ONO}, and σ^*_{ONO}.

For DMNA–Zn_{10}, we have employed ONIOM methodology using two layer QM:MM (Quantum Mechanics: Molecular Mechanics) and QM:QM combinations, in which one part of the cluster (mainly, DMNA and immediate binding site at the metal cluster) is treated at the CASSCF(14,11)/6-31G level of theory (QM), while the remainder of the cluster is treated either at the UFF level (MM) or at the MP2 (QM) level. The basic idea of ONIOM calculation results from the realization that for a large cluster photochemical processes are often localized only in a segment (called *active site*) of the cluster; the effect of the rest of the cluster on the active site can often be only steric or electrostatic. Therefore, the photochemical process, localized at the *active site* and being investigated, can be treated at an appropriate high-accuracy multiconfiguration QM method (e.g., CASSCF), while the remainder of the cluster can be treated only with a lower level of theory (e.g., MP2 QM or UFF MM). The 11 active orbitals, which are treated with CASSCF level for DMNA–Zn_{10} cluster, have been depicted in Fig. 2.

Vertical excitation energies are calculated by state-averaging over the ground and excited states with equal weights for each state. Critical points (minima and conical intersections) are optimized by using the algorithm implemented in Gaussian 09. The lowest energy point on the conical intersection seam, called lowest energy conical intersection, is optimized and localized using a projected gradient algorithm, as implemented in Gaussian 09. In this search, the energy of the excited state is minimized. At the same time, the energy difference between the excited state and the closest lower energy state is minimized. Minimum and transition states are optimized using Berny algorithm implemented in Gaussian 09. Stability of the structure is checked against frequency calculations. Transition state geometry exhibits one unstable normal mode of vibration, which is characteristic of the reaction pathway.

Some of the reaction pathways of DMNA–Zn_n clusters are explored through potential energy scanning. A relaxed potential

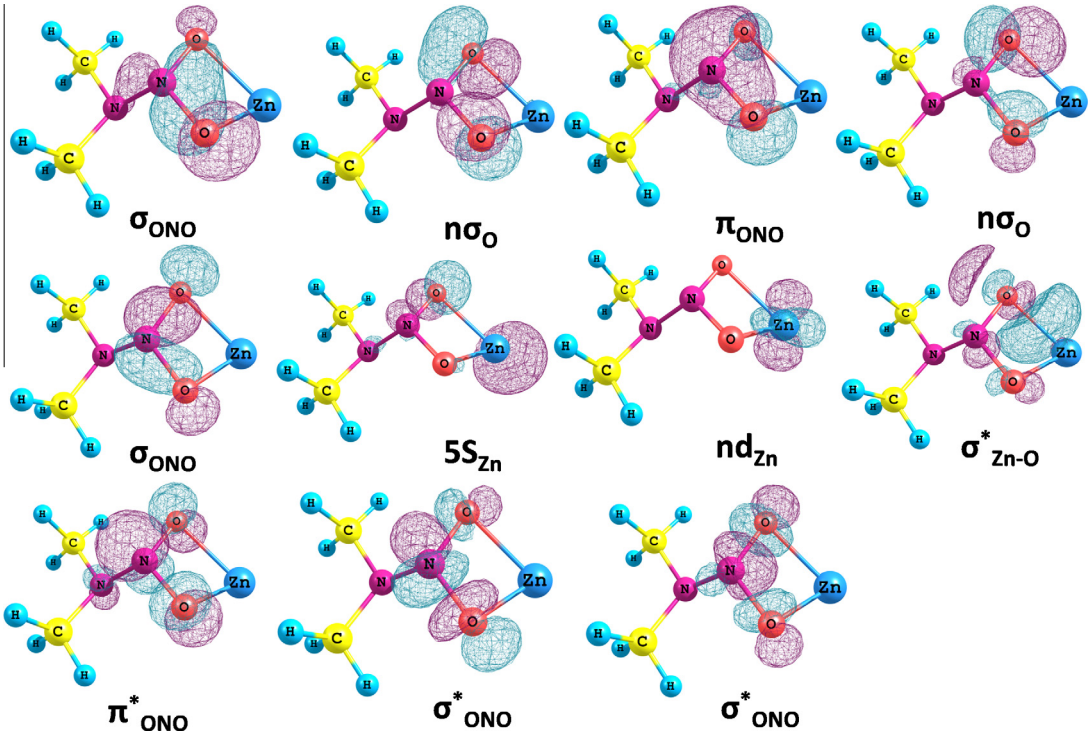

Fig. 1. Orbitals used in the active space in the CASSCF calculations for DMNA–Zn. The active space comprises 14 electrons, which are distributed in 11 active orbitals. Orbitals are computed at the CASSCF(14,11)/6-31G(d) level of theory.

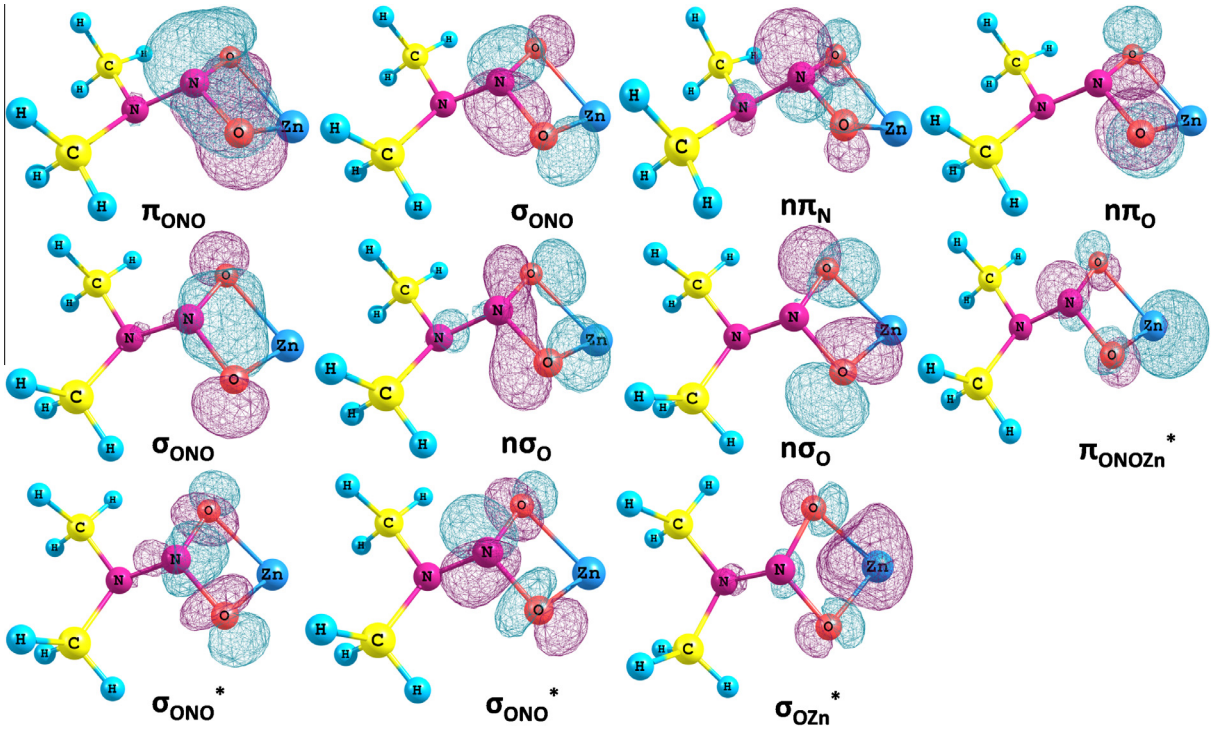

Fig. 2. Orbitals used in the active space in the ONIOM(CASSCF:UFF) calculations for DMNA–Zn_{10}. The active space comprises 14 electrons which are distributed in 11 active orbitals which are localized in the active site of DMNA–Zn_{10} cluster. The active site consists of DMNA molecule and one atop-Zn metal atom only. Orbitals are computed at the ONIOM(CASSCF/6-31G:UFF) level of theory.

energy scan is performed using Z-matrix by changing the scan variables (respective bond distance). The CASMP2 [15], which is multireference perturbation theory and which includes dynamic electron–electron correlation, is also employed to correct the CASSCF-computed energies.

3. Results and discussion

3.1. DMNA–Zn

The CASSCF-optimized ground state geometry (referred as $S_{0,Min1}$) of DMNA–Zn, as illustrated in Fig. 3, shows a non-planar N–NO_2 moiety, in which Zn atom is strongly bonded with O atoms. The dihedral angle, NNOO (in N–NO_2 active moiety), predicted at the CASSCF level of theory, is found to be ~133°. The MP2-optimized geometry exhibits similar non planar N–NO_2 moiety but with slightly different NNOO dihedral angle (~127°). Structures of isolated DMNA, optimized at the CASSCF and MP2 levels of theory, are also given in Fig. 3, for comparison. DMNA–Zn and isolated DMNA exhibit significantly different structures. The primary difference between DMNA–Zn and isolated DMNA structures is found to be in the N–NO_2 region: isolated DMNA features a planar N–NO_2 moiety, whereas, that of DMNA–Zn is non-planar due to interaction with the Zn atom. Furthermore, the N–O and the N–N bonds are elongated in DMNA–Zn as compared to that of isolated DMNA, which is depicted in Fig. 3.

The vertical excitation energies for DMNA–Zn, computed at the CASSCF(14,11)/6-31G(d) optimized Franck–Condon geometry (FC geometry at ground state minimum), are listed in Table 1. The calculations show that the two lowest lying excited electronic states (referred as $S_{1,FC}$ and $S_{2,FC}$, respectively) for DMNA–Zn possess vertical excitation energies of 4.01 and 4.87 eV, for the $S_{1,FC}$ and $S_{2,FC}$, respectively. The excitation to the $S_{1,FC}$ from $S_{0,Min1}$ corresponds to the electronic excitation from the bonding σ_{NO} and nonbonding nd_{Zn} orbitals to the antibonding σ^*_{NO} and σ^*_{ZnO} orbitals. Similarly, excitation to the $S_{2,FC}$ is associated with the electronic excitation from nonbonding $5S_{Zn}$ and nd_{Zn} to the antibonding π^*_{ONO}. As CASSCF theory does not include dynamic electron–electron correlation, often, it is preferred to recheck the computed vertical excitation energies of energetic molecules and clusters at the CASMP2 level of theory. Our previous work shows that for isolated DMNA and DMNA–Al clusters, dynamic correlation does not contribute to the CASSCF-computed energies significantly [12]. Nonetheless, here we have employed CASMP2 to include dynamic correlation

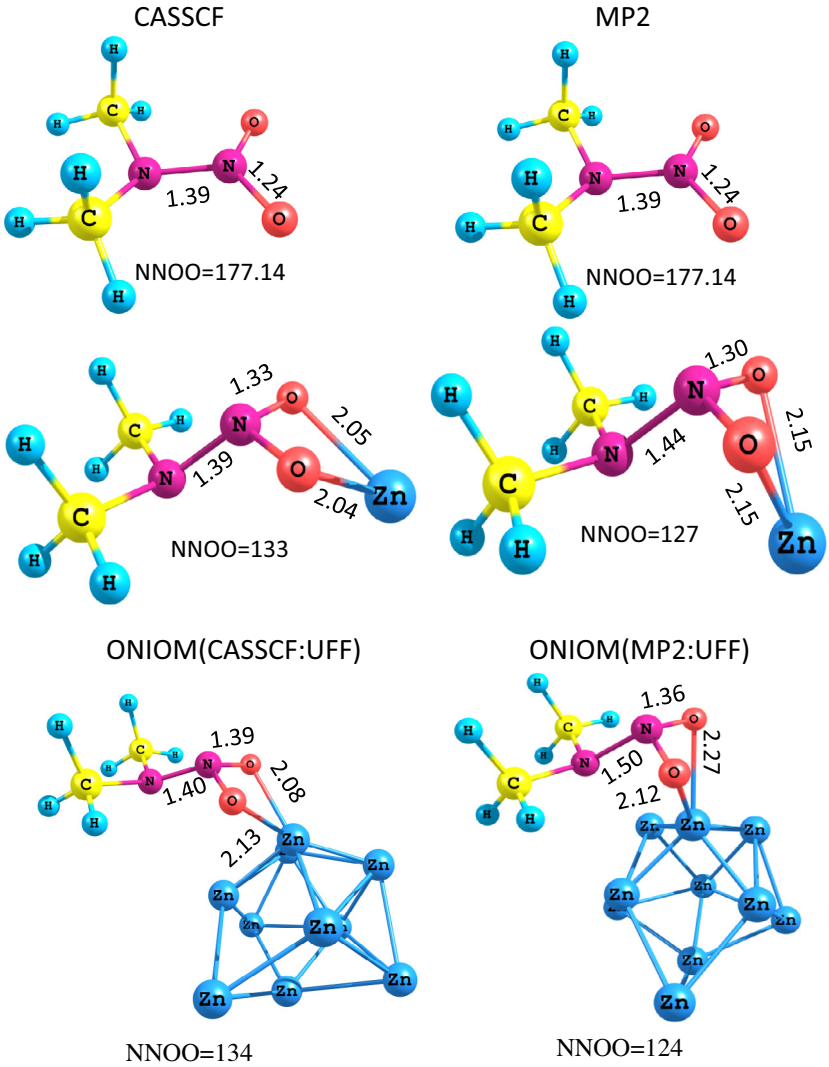

Fig. 3. Ground state optimized geometries of isolated DMNA and DMNA–Zn cluster, computed at the CASSCF(14,11)/6-31G(d), and that of DMNA–Zn_{10}, optimized at the ONIOM(CASSCF(14,11)/6-31G:UFF), are depicted. Relevant structural parameters are also given. Respective MP2-optimized geometries for isolated DMNA and DMNA–Zn and ONIOM(MP2/6-31G:UFF)-optimized geometry for DMNA–Zn_{10} are also illustrated for comparison.

Table 1
Relative energies (in eV) of different critical points, calculated with respect to the $S_{0,Min1}$ for DMNA–Zn, as computed at the CASSCF(14,11)/6-31G(d) and at the CASMP2(14,11)/6-31G(d) levels of theory. Vertical excitation energies are calculated using two different basis sets, namely 6-31G(d) and 6-311++G(d,p).

State/CI	ΔE (eV) CASSCF/ 6-31G(d)	ΔE (eV) CASMP2/ 6-31G(d)	ΔE (eV) CASSCF/ 6-311++G(d,p)
$S_{1,FC}$	4.01	3.10	4.06
$S_{2,FC}$	4.87	3.74	5.30
$(S_2/S_1)_{CI}$	3.49	2.35	
$(S_1/S_0)^a_{CI}$	1.50	1.21	
TS_1	2.82	1.90	
TS_2	0.12	0.10	
$(S_1/S_0)^b_{CI}$	−0.45	−1.43	
$S_{0,Min2}$	−2.92	−3.06	
$S_{0,Min3}$	−1.09	−1.22	
TS_3	−0.83	−0.92	
NO-elimination	−0.88	−0.70	
NO_2-elimination	2.47	2.72	

in the CASSCF-computed vertical excitation energies. Table 1 compares the vertical excitation energies, computed at the CASSCF and CASMP2 levels of theory with the same 6-31G(d) basis set, which features that the vertical excitation energies are reduced by a factor of ca. 0.75 upon inclusion of dynamic correlation. Due to this fact, we have recalculated energies of all the critical points on the ground and excited state potential energy surfaces at the CASMP2 level of theory for more reliable estimation of the relative energies to construct the potential energy surfaces of DMNA–Zn with adequate accuracy.

In order to judge the influence of different basis sets on the vertical excitation energies, we have also performed CASSCF calculations for vertical excitation energies of DMNA–Zn system with a very large basis set 6-311++G(d,p). Results are summarized in Table 1, which suggest that enlarging basis set in the present CASSCF calculation does not have significant effect on the vertical excitation energies. This is also found in our earlier works on DMNA and DMNA–Al clusters [12], evidencing the fact that in CASSCF-computations of energetic systems, once a good active space is selected, moderately large basis sets, such as 6-31G or 6-31G(d), can predict the relative excitation energies with adequate accuracy.

A number of critical points on the electronically excited and ground state PESs of DMNA–Zn are optimized at the CASSCF(14,11)/6-31G(d) level of theory. Respective optimized geometries are depicted in Fig. 4 with important bond lengths and bond angles. Present CASSCF level of theory identifies one conical intersection ($(S_2/S_1)_{CI}$) between S_2 and S_1 surfaces and two conical intersections ($(S_1/S_0)^a_{CI}$ and $(S_1/S_0)^b_{CI}$) between S_1 and S_0 surfaces. The $(S_2/S_1)_{CI}$ geometry does not change significantly as compared to the $S_{0,Min1}$ geometry (which is also FC point geometry on the S_2 surface). At the $(S_2/S_1)_{CI}$ point, both the N–N and the N–O bond distances in the N–NO_2 moiety are slightly increased by approximately 0.1 Å and the NNOO dihedral angle changes to 115°. DMNA–Zn geometry at the $(S_1/S_0)^a_{CI}$ also does not change significantly as compared to the FC geometry, except for NNOO dihedral angle. The NNOO dihedral angle is decreased to 105° at the $(S_1/S_0)^a_{CI}$. However, geometry of DMNA–Zn at the $(S_1/S_0)^b_{CI}$ point undergoes significant structural change, with elongation of N–N bond distance. The N–N bond distance is calculated to be 3.87 Å at the $(S_1/S_0)^b_{CI}$ point, which is more than 2.5 fold increase of N–N bond distance with respect to the FC point geometry.

On the S_1 surface, in addition to the conical intersections, one transition state (TS_1) associated with the N–N bond dissociation is also localized, which exhibits N–N bonds distance of 2.04 Å, as depicted in Fig. 4. On the ground potential energy surface, two isomers of DMNA–Zn, namely $S_{0,Min2}$ and $S_{0,Min3}$, are identified. Both the $S_{0,Min2}$ and $S_{0,Min3}$ geometries feature nitrite isomeric form; however, in the $S_{0,Min2}$ geometry two oxygen atoms are bonded with the Zn atom, whereas, at the $S_{0,Min3}$ point, only single oxygen atom is bonded with the Zn atom. All the critical points discussed above are internally connected with each other on the overall potential energy landscape of DMNA–Zn cluster, which is discussed below.

In order to explore the pathways, connecting different critical points on the PESs of DMNA–Zn, energy profile diagrams, which are obtained during optimization steps and using potential energy scanning, are carefully inspected. The energy profile diagrams with respect to the optimization steps, connecting FC points and related conical intersections on the S_2 and S_1 surfaces, as calculated at the CASSCF(14,11)/6-31G(d) level, are explicitly depicted in Fig. 5(a) and (b). As evident in these two figures, the decay paths connecting the FC point of the S_2 state to $(S_2/S_1)_{CI}$ on the S_2 surface and the same from the FC point of S_1 state to the $(S_1/S_0)^a_{CI}$ are found to be a downhill process. Structural evolution through these critical points (geometries at the critical points are illustrated in Fig. 4) suggests that after electronically exciting the DMNA–Zn cluster to the S_2 excited state potential energy surface, DMNA–Zn may experience an electronically nonadiabatic transition, first from the S_2 surface to the S_1 surface and then from the S_1 surface to the S_0 surface, through the $(S_2/S_1)_{CI}$ and the $(S_1/S_0)^a_{CI}$, respectively. This electronically nonadiabatic process does not change the DMNA–Zn structure significantly. However, on the S_1 surface, DMNA–Zn can also undergo N–N bond dissociation through the TS_1 and can follow another electronically nonadiabatic transition from S_1 surface to the S_0 surface through the $(S_1/S_0)^b_{CI}$, which finally renders the N–N bond dissociation. Fig. 5(c) features a downhill pathway (with respect to the optimization steps), connecting the TS_1 to the $(S_1/S_0)^b_{CI}$, as calculated at the CASSCF(14,11)/6-31G(d) level.

A schematic one dimensional plot of the multidimensional electronic PESs (S_0, S_1, and S_2) of DMNA–Zn with structures of different critical points is depicted in Fig. 6, to summarize the results discussed above. Upon electronic excitation of DMNA–Zn to the FC point of the S_2 state, DMNA–Zn can follow a barrierless internal conversion pathway from the FC point of the S_2 state to the $(S_2/S_1)_{CI}$, and then from the $(S_2/S_1)_{CI}$ to the $(S_1/S_0)^a_{CI}$. The DMNA–Zn cluster can also undergo N–N bond dissociation on the S_1 surface. If the DMNA–Zn remains on the S_1 surface and undergoes N–N bond dissociation on the same surface, then it can undergo another nonadiabatic transition from the upper S_1 surface to the lower S_0 surface through the $(S_1/S_0)^b_{CI}$. A large N–N bond distance (3.87 Å) is predicted at the $(S_1/S_0)^b_{CI}$. This pathway ultimately produces a very stable dimethyl (μ^2-nitro) amine zinc complex ($S_{0,Min2}$) on the ground electronic potential energy surface. The unusual stability of the $S_{0,Min2}$ (−3.06 eV with respect to $S_{0,Min1}$, calculated at the CASMP2/6-31G(d)) is due to formation of strong Zn–O bonds. Thereafter, DMNA–Zn can undergo a Zn–O bond dissociation through TS_3, which is associated with activation barrier of 2.14 eV (computed at the CASMP2/6-31G(d)) with respect to the $S_{0,Min2}$. The pathway, related to the Zn–O bond dissociation from the $S_{0,Min2}$, which finally results in formation of $S_{0,Min3}$, is explicitly computed using potential energy scanning and is depicted in Fig. 5(d). Note that although the Zn-O bond dissociation pathway possesses an activation barrier of 2.14 eV with respect to the $S_{0,Min2}$, this reaction channel is exothermic with respect to the $S_{0,Min1}$.

Upon formation of the $S_{0,Min3}$, both the NO_2 and the NO elimination channels can be opened up; however, the NO elimination limit is calculated to be only 0.52 eV (CASMP2) with respect to the $S_{0,Min3}$, while that of NO_2 elimination is computed to be 3.94 eV (CASMP2) with respect to the $S_{0,Min3}$. At the CASSCF level of theory, the NO and NO_2 dissociation limits have been evaluated by

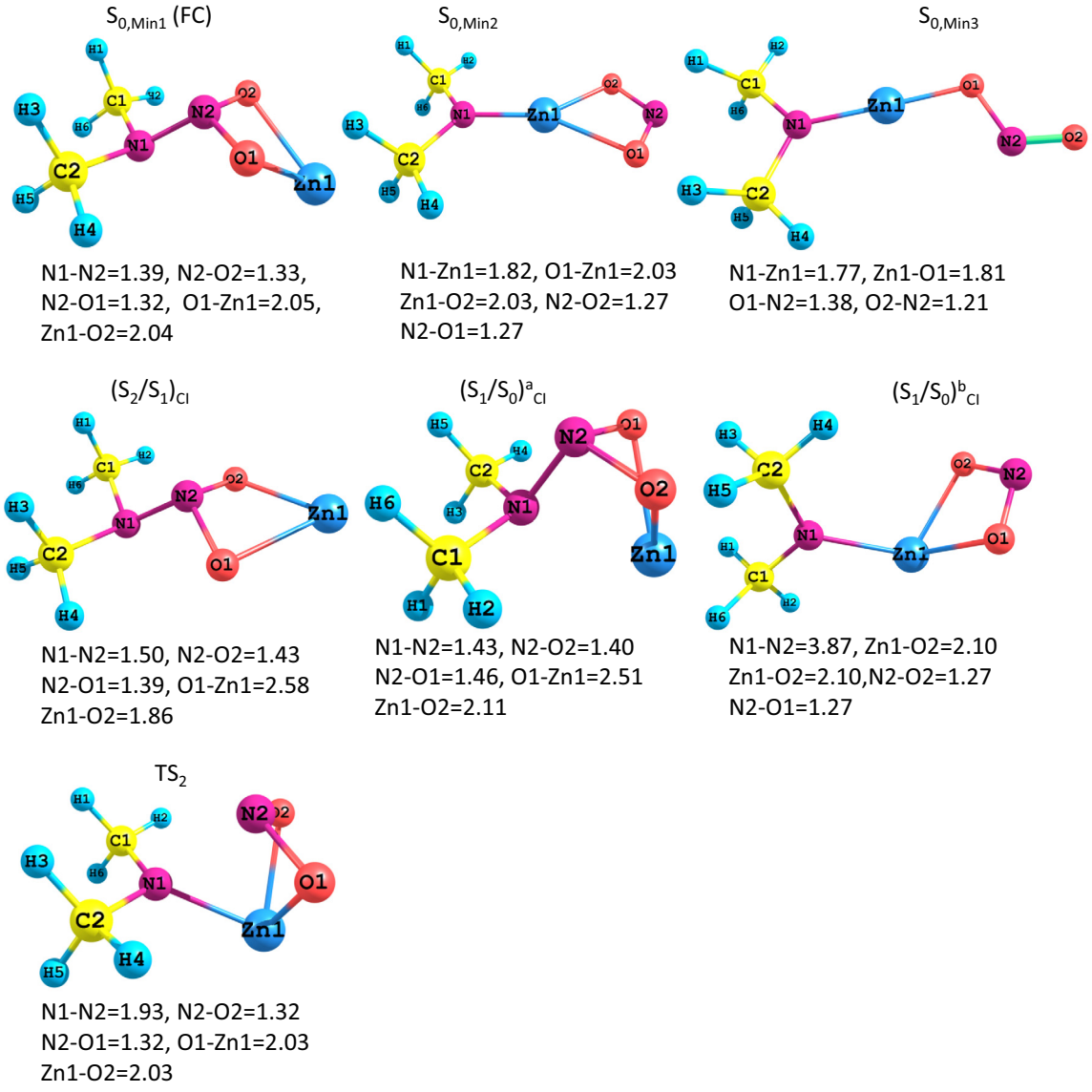

Fig. 4. Optimized geometries of DMNA–Zn at different critical points on the electronically excited as well as ground state PESs, as revealed at the CASSCF(14,11)/6-31G(d) level of theory.

optimizing the geometry, in which the NO or the NO_2 moiety is placed at a distance of ~10 Å from remainder of the cluster.

Therefore, two possible electronically non-adiabatic decomposition schemes (as also illustrated in Fig. 6) for DMNA–Zn are as follows:

(1) Path 1: DMNA–Zn $(S_{2,FC}) \rightarrow (S_2/S_1)_{CI} \rightarrow (S_1/S_0)^a_{CI} \rightarrow TS_1 \rightarrow (S_1/S_0)^b_{CI} \rightarrow$ DMNA–Zn $(S_{0,Min2}) \rightarrow TS_3 \rightarrow$ nitrite $(S_{0,Min3}) \rightarrow$ NO.
(2) Path 2: DMNA–Zn $(S_{2,FC}) \rightarrow (S_2/S_1)_{CI} \rightarrow (S_1/S_0)^a_{CI} \rightarrow (S_1/S_0)^b_{CI} \rightarrow$ DMNA–Zn $(S_{0,Min2}) \rightarrow TS_3 \rightarrow$ nitrite $(S_{0,Min3}) \rightarrow$ NO.

Both decomposition pathways stated above, however, undergo through a common intermediate $S_{0,Min2}$ on the ground state potential energy surface. Furthermore, for both mechanisms, the NO elimination limit is computed to be −0.70 eV (CASMP2) with respect to the $S_{0,Min1}$ geometry, which implies that the overall decomposition of DMNA–Zn through NO elimination is exothermic in nature.

In the context of excited electronic state decomposition of DMNA–Zn, it is relevant to recollect the decomposition pathways for isolated DMNA [11(a)] and DMNA–Al clusters [12]. Previous CASSCF calculations show that the DMNA–Al cluster dissociates through several steps: first, Al–O bond dissociation, then N–N bond dissociation followed by isomerization and finally NO elimination. One noticeable difference in decomposition pathways between DMNA–Zn and DMNA–Al is that the first decomposition step for DMNA–Zn is N–N bond dissociation, whereas, Al–O bond dissociation is the initial decomposition step for DMNA–Al. On the other hand, isolated DMNA exhibits decomposition pathway, involving isomerization followed by NO elimination. Overall electronically nonadiabatic reactions of both DMNA–Al and DMNA–Zn are predicted to be exothermic (approximately by −0.7 eV); however, isolated DMNA features endothermic (by +1.69 eV) electronically nonadiabatic reaction pathways.

3.2. DMNA–Zn_{10}

Exploring excited electronic state PESs of large clusters (or adsorbate-covered metal cluster surfaces) is pretty daunting task [5,17]. This is not directly feasible using only conventional quantum mechanical methodologies which can successfully describe

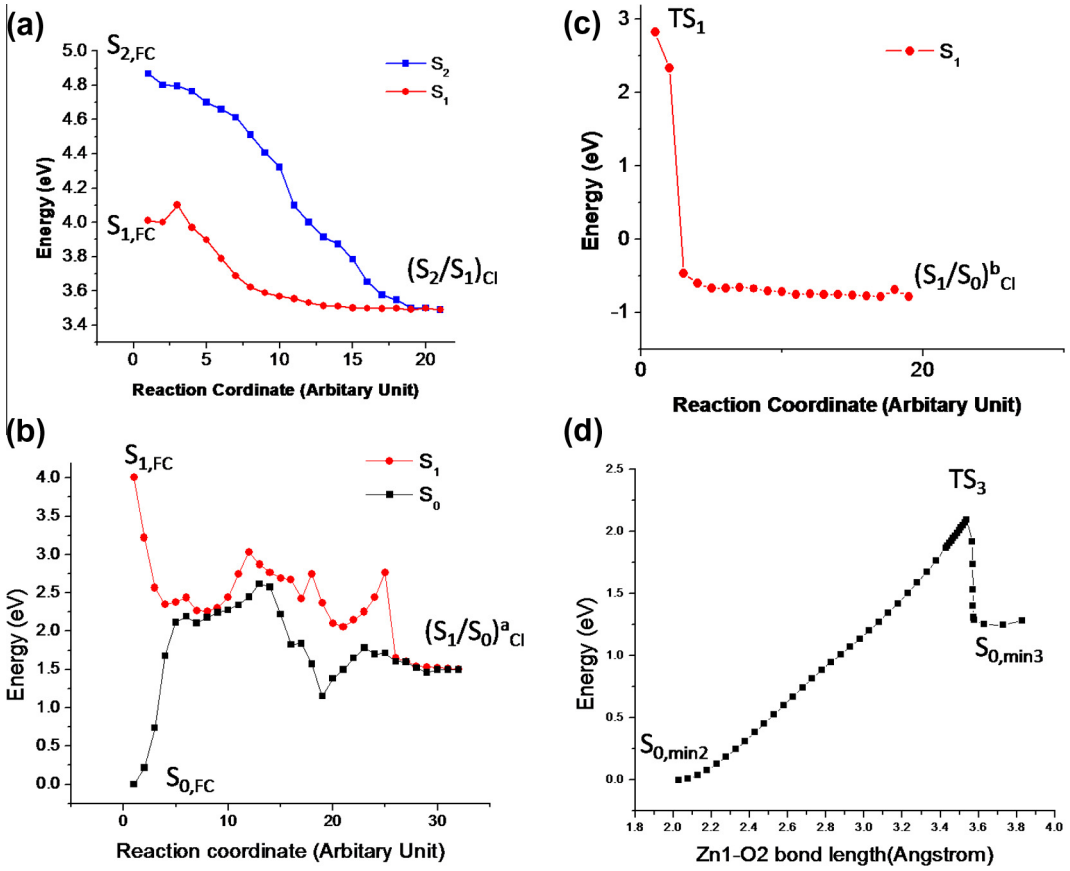

Fig. 5. Energy profile diagrams obtained during optimization steps, computed at the CASSCF(14,11)/6-31G(d) for DMNA–Zn: (a) from the $S_{2,FC}$ and $S_{1,FC}$ to the $(S_2/S_1)_{CI}$; (b) from the $S_{1,FC}$ and $S_{0,FC}$ to the $(S_1/S_0)^a_{CI}$; (c) from the TS_1 to the $(S_1/S_0)^b_{CI}$; (d) The path from the $S_{0,Min2}$ to the $S_{0,Min3}$ via TS_3 which is obtained using potential energy scanning along Zn1–O2 bond distance.

an electronically excited state of small molecule with adequate accuracy. In general, multiconfiguration-based *ab initio* QM methods, such as complete active space self-consistent field (CASSCF) and CAS perturbation theories (e.g., CASMP2), are very appropriate for exploring excited electronic state potential energy surfaces of small molecules. This is also evident in case of DMNA–Zn. However, they are way too expensive to apply to large systems, like DMNA–Zn_{10}. Here we note that DMNA–Zn_{10} cluster is not large in the sense of number of atoms; instead, it is large because of its very large active space which needs to be taken into account in the CASSCF computations, which makes it impossible to carry out reliable calculations of electronically nonadiabatic processes of DMNA–Zn_{10}. Only recently, a few reports, based on first principle calculations, have been documented in literature, which demonstrate potential application of hybrid methodologies in studying localized excited electronic states for large systems [5,17]. In the hybrid formalism, a representative region (e.g., adsorbate with the adsorption site on metal surface), is treated by an accurate quantum chemical method, suitable for the computation of excited electronic states (e.g., CASSCF), and the influence of the remainder of the system is computed via less expensive methods (e.g., UFF-MM or low level QM methods). "Our own N-layered integrated molecular orbital and molecular mechanics" (ONIOM) method is one of the efficient hybrid schemes, employing which successful exploration of the electronically nonadiabatic processes of large energetic molecules, such as RDX, has been performed, recently by Bhattacharya et al. [5]. To the best of our knowledge, there has been no effort made so far to utilize this method, coupled with the CASSCF methodology, to calculate the local electronically excited states of energetic molecules (including the one discussed in the present article) at any metal cluster surface. Here we have selected Zn_{10} cluster for our present computational study.

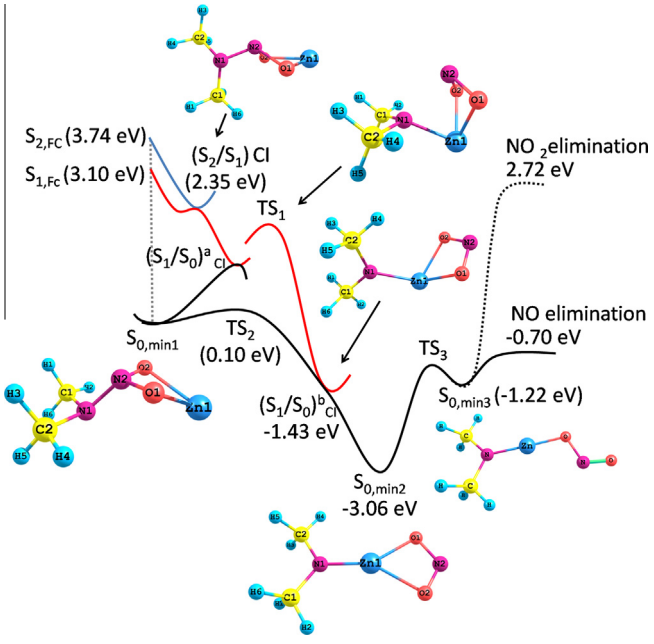

Fig. 6. One dimensional schematic plot of the multidimensional electronic potential energy surfaces of DMNA–Zn complex, computed at the CASMP2(14,11)/6-31G(d) level of theory.

The optimized geometry of Zn_{10} cluster is illustrated in Fig. 7, as obtained at the B3LYP/6-31G level of theory. Similar structure of Zn_{10} was also previously predicted by Tachikawa et al. at the MP2/LANL2DZ level of theory [13]. Undoubtedly, DMNA molecule can bind the Zn_{10} surface via different possible binding sites, such as atop, bridge-head, three-fold-hollow sites, and, etc., which are present at the surface of Zn_{10} cluster. However, to obtain simplest picture, here, we have considered only atop binding site for the calculation and therefore, electronic excitation is assumed to be localized entirely at the atop-Zn–DMNA moiety. The atop-Zn–DMNA moiety is selected to be the *active site* in the ONIOM calculation, which is treated at the CASSCF level of theory. This *active site* is depicted with balls in Fig. 7. Atoms in wireframe, illustrated in the same figure, are treated with the low level computational methodology. In our present calculation, we have used two different low levels of theory, which include UFF (MM) and MP2/6-31G (QM). The combination of CAS and UFF is called QM:MM combination and that of CAS:MP2 is QM:QM combination. Furthermore, during ONIOM(CASSCF:UFF) optimizations, we have relaxed the *active site*, which includes DMNA molecule and only atop-Zn atom of Zn_{10} cluster; the rest of Zn atoms in Zn_{10} cluster are frozen in order to retain the overall metal cluster structure during decomposition of DMNA–Zn_{10} cluster following electronic excitation. This restricted geometry optimization enables us to focus only on the electronically nonadiabatic chemistry of atop-Zn–DMNA moiety in presence of Zn_{10} cluster.

The ONIOM(CASSCF:UFF)-optimized ground state geometry ($S_{0,Min1}$) of DMNA–Zn_{10} cluster, is illustrated in Fig. 3. Structure of DMNA–Zn_{10} optimized at the ONIOM(MP2/6-31G:UFF) level of theory, is also given in the same figure, for comparison. The primary difference between the ONIOM-CASSCF- and ONIOM-MP2-optimized structures of DMNA–Zn_{10} is found in the NNOO dihedral angles: 134° and 124° are obtained, respectively. However, both structures show a non-planar N–NO_2 moiety.

The vertical excitation energies for DMNA–Zn_{10}, computed at the ONIOM(CASSCF(14,11)/6-31G:UFF) optimized FC geometry, are listed in Table 2, which shows that the vertical excitation energy associated with the first excited state is 2.54 and 4.27 eV. On the other hand, vertical excitation energy of DMNA–Zn_{10} at the ONIOM(CASSCF(14,11)/6-31G:MP2/6-31G) level of theory predicts 2.25 and 3.16 eV, respectively for the S_1 and S_2 excited states. At this point, it is not possible to compare these computed

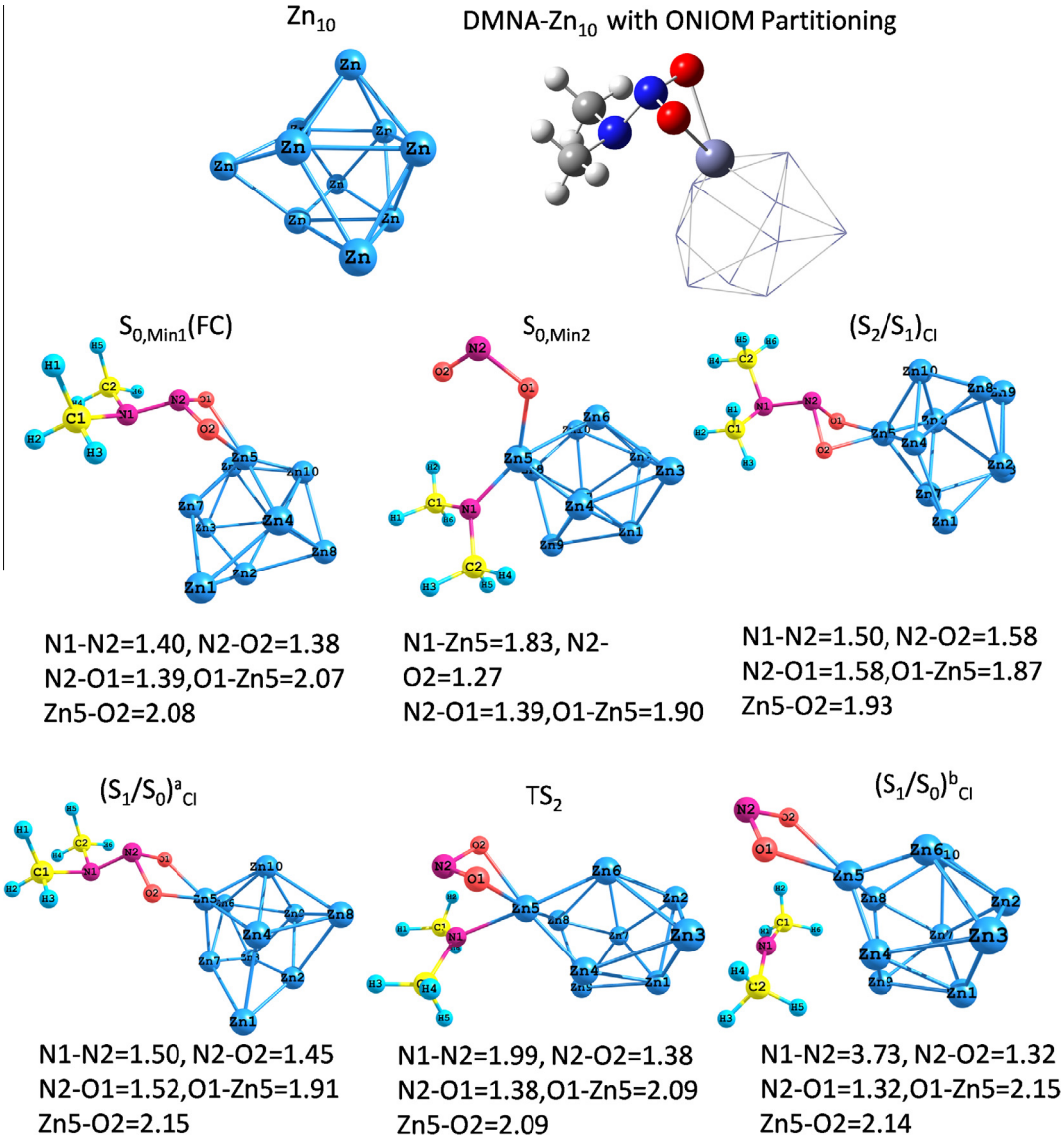

Fig. 7. Optimized geometries of DMNA–Zn_{10} obtained at different critical points on the excited as well as ground state potential energy surfaces, which are computed at the ONIOM(CASSCF(14,11)/6-31G:UFF) level of theory. The Zn_{10} cluster is optimized at the B3LYP/6-31G level of theory.

Table 2
Relative energies (in eV) of different critical points, calculated relative to the $S_{0,Min1}$ for DMNA–Zn_{10} cluster, are given. Relative energies are computed at the ONIOM(CASSCF(14,11)/6-31G:UFF) and the ONIOM(CASSCF(14,11)/6-31G:MP2/6-31G) levels of theory.

State/CI	ΔE (eV) ONIOM (CAS/6-31G:UFF)	ΔE (eV) ONIOM (CAS/6-31G:MP2/6-31G)
$S_{1,FC}$	2.54	2.25
$S_{2,FC}$	4.27	3.16
$(S_2/S_1)_{CI}$	3.34	2.01
$(S_1/S_0)^a_{CI}$	1.67	1.30
$(S_1/S_0)^b_{CI}$	1.60	−0.21
TS_1	5.09	2.50
TS_2	4.63	0.98
$S_{0,Min3}$	−1.44	−1.92
NO-elimination	2.63	−1.74
NO_2-elimination	4.67	2.60

vertical excitation energies with the experimental observations because electronic absorption spectrum of DMNA in presence of Zn clusters is unknown. However, these results can be compared with DMNA–Zn and DMNA–Zn_2 results, for which pure quantum mechanical calculation at the CASSCF level of theory can be performed. Going from monomeric Zn to dimeric Zn, we notice that the vertical excitation energies associated with lowest lying excited electronic states are reduced. The vertical excitation energies for DMNA–Zn_2, computed at the CASSCF(14,11)/6-31G(d) optimized FC geometry, are calculated to be 3.28 and 4.81 eV, respectively. The two lowest lying excited electronic states for DMNA–Zn, on the other hand, exhibit vertical excitation energies of 4.01 and 4.87 eV, respectively. It is, therefore, expected that the excitation energy for DMNA–Zn_{10} (which contains 10 Zn atoms) should be further reduced as compared to that of DMNA–Zn_2. Therefore, to the best of our understanding, ONIOM(CAS:MP2) predicts more reliable excitation energies as compared to ONIOM(CAS:UFF) for DMNA–Zn_{10}. This conclusion is technically justified as at the ONIOM(CAS:UFF) level of theory, in which the low level of theory is UFF molecular mechanics, the DMNA–Zn_{10} system is treated with molecular mechanics force field which may render oversimplified picture of interactions within metal cluster frameworks; instead, a pure QM:QM combination in ONIOM calculation is more appropriate for systems containing metal clusters. However, it is also important to remember that a QM:QM combination in ONIOM calculation consumes high computational time, as compared to a QM:MM combination. Therefore, in the present work, to balance the computational time and the accuracy of the calculations, we have used ONIOM(CAS:UFF) level of theory to optimize different critical points on the excited and ground state potential energy surfaces of DMNA–Zn_{10} and then energies of all critical points recalculated at the ONIOM(CAS:MP2) level of theory.

The ONIOM(CAS:UFF) level of theory identifies a number of critical points on the excited and ground state potential energy surfaces of DMNA–Zn_{10} cluster, including two conical intersections between the S_1 and S_0 surfaces [$(S_1/S_0)^a_{CI}$ and $(S_1/S_0)^b_{CI}$], one conical intersection between the S_2 and the S_1 surfaces [$(S_2/S_1)_{CI}$], one N–N bond dissociation transition state (TS_1) on the S_1 surface, and other minima on the S_0 surface. The optimized geometries at these critical points are depicted in Fig. 7. A schematic one dimensional plot of the multidimensional electronic PESs (S_2, S_1 and S_0) of DMNA–Zn_{10} with ONIOM(CAS:MP2)-computed energies is illustrated in Fig. 8. This PES diagram for DMNA–Zn_{10} suggests that following electronic excitation of DMNA–Zn_{10} to the S_2 surface, the cluster can undergo electronically nonadiabatic transition from the upper S_2 state to the lower S_1 state through the $(S_2/S_1)_{CI}$ conical intersection. This nonadiabatic surface jump is quite similar in nature to that of DMNA–Zn cluster; however, the relative energies (with

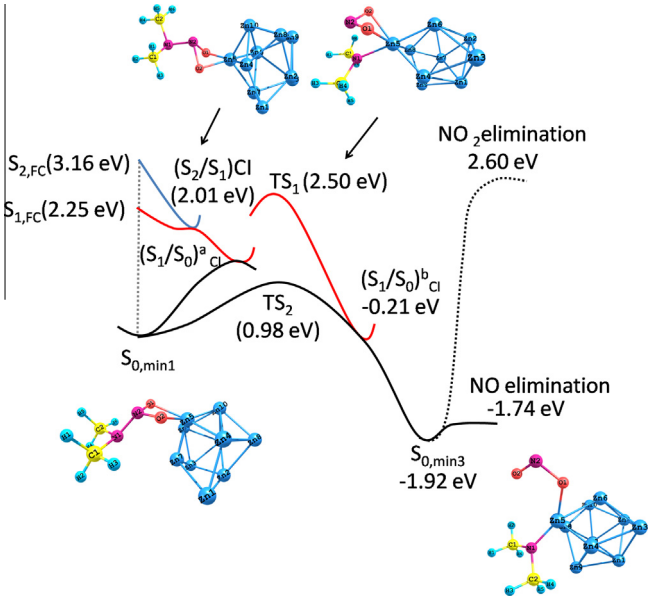

Fig. 8. One dimensional schematic plot of the multidimensional electronic potential energy surfaces of DMNA–Zn_{10} complex, computed at the ONIOM(CASSCF(14,11)/6-31G:MP2/6-31G) level of theory.

respect to the $S_{0,Min1}$) of the critical points for DMNA–Zn_{10} is found to reduce by a factor of ca. 0.8 as compared to that of DMNA–Zn.

Similar to DMNA–Zn results, on the S_1 surface, DMNA–Zn_{10} can also open up two possible channels: one associated with N–N bond dissociation through (TS_1) followed by nonadiabatic transition from upper S_1 state to the lower S_0 state through the $(S_1/S_0)^b_{CI}$ and another connected with direct nonadiabatic transition from the S_1 to the S_0 surface through the $(S_1/S_0)^b_{CI}$. If DMNA–Zn_{10} follows the first channel, N–N bond dissociation occurs on the S_0 surface, but if DMNA–Zn_{10} follows the second channel, N–N bond dissociation occurs on the S_1 excited state surface. Our calculation predicts that both channels can be opened up as long as DMNA–Zn_{10} is electronically excited above 2.5 eV.

On the S_0 ground electronic surface, the $(S_1/S_0)^b_{CI}$ is found to be directly connected with the $S_{0,Min3}$, which features a structure (as depicted in Fig. 7), resembling nitrite isomeric form, in which only one oxygen atom of NO_2 group is attached with atop-Zn atom. Similar intermediate was also found for DMAN–Zn cluster; however, the primary difference between the $S_{0,Min3}$ intermediates of DMNA–Zn and DMNA–Zn_{10} is that DMNA–Zn possesses planar N–Zn–ONO moiety, whereas, DMNA–Zn_{10} exhibits non-planar N–Zn–ONO moiety. The planarity of N–Zn–ONO moiety is broken in case of DMNA–Zn_{10} cluster because of steric effect of Zn_{10} cluster, which is absent in DMNA–Zn system. Subsequent NO and NO_2 elimination pathways for DMNA–Zn_{10} are also explored and the results are summarized in Table 2. In concordance with DMNA–Zn system, NO elimination is also found to be the lowest energy pathway of dissociation for DMNA–Zn_{10} cluster. Here, it is also interesting to note that, when we attempted to optimize a structure for DMNA–Zn_{10} similar to $S_{0,Min2}$ geometry (where two oxygen atoms are bonded with Zn atom) of DMNA–Zn, we always obtained $S_{3,Min3}$ structure. After an exhaustive search, we confirm that the $S_{0,Min2}$ intermediate does not exist for DMNA–Zn_{10} cluster.

Thus, two possible electronically nonadiabatic decomposition reactions of DMNA–Zn_{10} can be written as:

(a) Path 1: DMNA–Zn_{10} ($S_{2,FC}$) → $(S_2/S_1)_{CI}$ → TS_1 (N–N bond dissociation) → $(S_1/S_0)^b_{CI}$ → nitrite ($S_{0,Min3}$) → NO.
(b) Path 2: DMNA–Zn_{10} ($S_{2,FC}$) → $(S_2/S_1)_{CI}$ → $(S_1/S_0)^a_{CI}$ → nitrite ($S_{0,Min3}$) → NO.

4. Conclusions

In this present article, we have addressed the electronically nonadiabatic decomposition mechanisms of dimethylnitramine (DMNA) in presence of Zn atom and Zn_{10} cluster. To understand the role of Zn atoms/cluster in the overall electronically nonadiabatic decomposition mechanisms of Zn–containing DMNA, we have explored the electronically nonadiabatic potential energy surfaces of DMNA–Zn and DMNA–Zn_{10} clusters. The electronically excited state surfaces for DMNA–Zn are explored at the CASSCF(14,11)/6-31G(d) level of theory; whereas, ONIOM(CASSCF(14,11)/6-31G:UFF) and ONIOM(CASSCF(14,11)/6-31G:MP2/6-31G) are employed to investigate the excited electronic state PESs of relatively large DMNA–Zn_{10} cluster. This is the first report of electronically nonadiabatic processes of large metal cluster-containing energetic molecules.

The electronic potential energy surfaces (S_0, S_1, and S_2) of all DMNA–Zn cluster systems are found to be highly coupled, yielding various conical intersections between two electronic potential energy surfaces. This offers DMNA–Zn and DMNA–Zn_{10} a direct minimum energy non-adiabatic pathway from upper electronic states to lower ground state. Both DMNA–Zn and DMNA–Zn_{10} clusters can undergo electronically nonadiabatic transition from the upper S_2 or S_1 excited states to the ground electronic S_0 surface. Both can undergo N–N bond dissociation on the S_1 surface or on the S_0 surface; however, the $S_{0,Min2}$ intermediate, which is present for DMNA–Zn, does not exist for DMNA–Zn_{10}. Furthermore, thermodynamically exothermic NO elimination is found to be the final minimum energy decomposition channel for both DMNA–Zn and DMNA–Zn_{10} clusters. Isolated DMNA, on the other hand, exhibits endothermic NO elimination as minimum energy decomposition channel. Therefore, electronically nonadiabatic decomposition behavior of DMNA in presence of various Zn clusters changes significantly.

Conflict of interest

There is no conflict of interest.

Acknowledgments

Indian Institute of Science (IISc, Part-2A-XII Plan 12-0201-0243-01-403), ISRO-IISc Space Technology Cell (ISTC/CIP/ATB/0333), and DST-Nano Mission (SR/NM/NS-1117/2013) are gratefully acknowledged for the financial support of this research.

References

[1] G.A. Olah, D.R. Squire, Chemistry of Energetic Materials, Academic Press, 1991.
[2] S.N. Bulusu, Chemistry and Physics of Energetic Materials, Springer Science and Business Media, 1990.
[3] (a) D. Thompson, T. Brill, R. Shaw, Overviews of Recent Research on Energetic materials, World Scientific, New Jersey, 2004;
(b) J.R. Sabin, Energetic Materials, Advances in Quantum Chemistry, vol. 69, Academic Press, 2014.
[4] (a) E.R. Bernstein, Role of Excited Electronic States in the Decomposition of Energetic Materials, in: D. Thompson, T. Brill, R. Shaw (Eds.), Overviews of Recent Research on Energetic materials, World Scientific, New Jersey, 2004;
(b) F.E. Williams, Adv. Chem. Phys. 21 (1971) 289;
(c) J. Sharma, B.C. Beard, M. Chaykovsky, J. Phys. Chem. 95 (1991) 1209;
(d) J. Gilman, J. Philos. Mag. B 71 (1995) 1057;
(e) M.M. Kuklja, B.P. Aduev, E.D. Aluker, V.I. Krasheninin, A.G. Krechetov, A.Y. Mitrofanov, J. Appl. Phys. 89 (2001) 4156;
(f) H.M. Windawi, S.P. Varma, C.B. Cooper, F. Williams, J. Appl. Phys. 47 (1976) 3418.
[5] A. Bhattacharya, E.R. Bernstein, J. Phys. Chem. A 115 (2011) 4135.
[6] A. Bhattacharya, Y.Q. Guo, E.R. Bernstein, Acc. Chem. Res. 43 (2010) 1476.
[7] (a) P. Politzer, P. Lane, M.E. Grice, J. Phys. Chem. A 105 (2001) 7473;
(b) M.T. Swihart, L. Catoire, Combust. Flame 121 (2000) 210;
(c) K.K. Kuo, G.A. Risha, B.J. Evans, E. Boyer, Mater. Res. Soc. Symp. Proc. 800 (2003) 3.
[8] M.-A. Xue, J.-H. Wu, S. Ye, D. Hu, X.-D. Yang, Y.-P. Wang, W.-J. Zhu, C.-B.J. Li, J. Phys. D: Appl. Phys. 41 (2008) 04550.
[9] E.P. Snyder, H. Seltz, J. Am. Chem. Soc. 67 (1945) 683.
[10] S.George Parks, Hablutzel E. Charles, Webster E. Lawrence, J. Am. Chem. Soc. 49 (1927) 2792–2795.
[11] (a) A. Bhattacharya, Y.Q. Guo, E.R. Bernstein, J. Phys. Chem. A 113 (2009) 811;
(b) M.J. McQuaid, A.W. Miziolek, R.C. Sausa, C.N. Merrow, J. Phys. Chem. 95 (1991) 2713;
(b) J.C. Mialocq, J.C. Stephenson, Chem. Phys. Lett. 123 (1986) 390;
(c) J.C. Mialocq, J.C. Stephenson, Chem. Phys. 106 (1986) 281;
(d) G.W. Lemire, J.B. Simeonsson, R.C. Sausa, Anal. Chem. 65 (1993) 529;
(e) J.B. Simeonsson, G.W. Lemire, R.C. Sausa, Appl. Spectrosc. 11 (1993) 1907.
[12] A. Bera, A. Bhattacharya, J. Chem. Sci. (2014). accepted for publication.
[13] K. Iokibe, H. Tachikawa, K. Azumi, J. Phys. B At. Mol. Opt. Phys. 40 (2007) 427.
[14] (a) S. Dapprich, I. Komáromi, K.S. Byun, K. Morokuma, M.J.J. Frisch, Mol. Struct. (Theochem) 462 (1999) 1;
(b) T. Vreven, K. Morokuma, Ö. Farkas, H.B. Schlegel, M.J. Frisch, J. Comput. Chem. 24 (2003) 760;
(c) T. Vreven, K. Morokuma, Annu. Rep. Comput. Chem. 2 (2006) 35.
[15] J.J. McDouall, K. Peasley, M.A. Robb, Chem. Phys. Lett. 148 (1988) 183.
[16] M.J. Frisch, G.W. Trucks, H.B. Schlcgl, et al., GAUSSIAN 09, Gaussian Inc., Pittsburgh, PA, 2009.
[17] (a) M.J. Bearpark, F. Ogliaro, T. Vreven, M. Boggio-Pasqua, M.J. Frisch, S.M. Larkin, M. Morrison, M.A.J. Robb, Photochem. Photobiol. A Chem. 190 (2007) 207;
(b) M.J. Bearpark, S.M. Larkin, T. Vreven, J. Phys. Chem. A 112 (2008) 7286;
(c) T. Klüner, N. Govind, Y.A. Wang, E.A. Carter, Phys. Rev. Lett. 86 (2001) 5954.